INTEGRATION OF A DUCTED HYDROGENERATOR IN THE HULL OF THE MAXI-TRIMARAN SPINDRIFT 2

L. Mazas and **D. Barcarolo,** HydrOcean, France, loic.mazas@hydrocean.fr, daniel.barcarolo@hydrocean.fr
Y. Troalen, Spindrift racing**,** France, contact@spindrift-racing.com
M. Michou, Watt&Sea, France, matthieu.michou@wattandsea.com

Energy production has become one of the major issues aboard sailing yachts today. Indeed, the autopilot, the security devices, navigation systems, media devices, etc. require important amounts of energy. In order to prepare the maxi-trimaran Spindrift 2 to beat the Jules Verne Trophy, Spindrift racing's team decided to implant a hydrogenerator in the hull. The device would help to produce electric energy and thus carry less fuel aboard.
In this article, the work performed to design the hydrogenerator is detailed. Three geometries of ducts were designed and evaluated in CFD with an actuator-disk model. Results in terms of mass flow rate, additional drag and uniformity of the wake field map enabled to draw an optimized design. Simulations on that final design gave the wake field maps, necessary to design the turbine's blades. Then, the whole hydrogenerator was evaluated with rotating turbine in CFD, in order to predict the power at 15, 25 and 35 kts. Finally, Spindrift racing team built the hydrogenerator in composite materials, integrated it to the trimaran and tested it during sea trials. The relative difference on the useful power between experimental measurements and CFD prediction at 25 kts were 16%. On the range of speed considered, the trends were respected.
This work has been conducted in collaboration with 3 privately held companies: Spindrift racing, owner of the boat and final user, HydrOcean, specialist in CFD and hydrodynamics and Watt&Sea, designer of the blades and generator.

NOMENCLATURE

η_e	Electrical efficiency (-)
η_h	Hydraulic efficiency (-)
ρ	Density of water (kg.m^{-3})
AD	Actuator-disk
n	Rotation rate of the turbine (rpm)
P_s	Shaft power (W)
P_u	Useful power (W)
Q_{AD}	Torque of the actuator-disk (N.m)
Q_{turb}	Torque of the turbine (N.m)
Q_m	Mass flow rate (kg.s^{-1})
R_{out}	Duct outer radius (m)
T_{AD}	Thrust of the actuator-disk (N)
T_{turb}	Thrust of the turbine (N)
U_a	Axial velocity in the duct (m/s)
U_r	Radial velocity in the duct (m/s)
U_θ	Tangential velocity in the duct (m/s)
U_{tot}	Total velocity in the duct (m/s)
V_{AD}	Mean velocity with actuator-disk (m/s)
V_{turb}	Mean velocity with turbine (m/s)

1 INTRODUCTION

This paper presents the study performed in order to design a ducted hydrogenerator in the hull of maxi-trimaran Spindrift 2. This work was performed thanks to Computational Fluid Dynamics (CFD) simulations.

The objective of the study was to design a hydrogenerator that would deliver electrical power thanks to a turbine, set in rotation by the water inflow and connected to a generator producing electricity. The goal was to obtain 300 W of useful electrical power generated when the trimaran sails at 25 kts.
This paper is organised as follows: first, design a suitable geometry for the duct, then design a turbine adapted to the flow in the duct, and finally predict the power delivered by the hydrogenerator.
After the numerical study, Spindrift racing team built the device and tested it during sea trials. Measurements were logged and compared to CFD predictions. Finally, possible ways of improving the system are mentioned.

2 MODEL SETUP

2.1 GEOMETRY

In the CFD simulations, only the central hull of the maxi-trimaran was modelled, without appendages. As the daggerboard is located aft the hydrogenerator, it was assumed that it would not influence the flow going through the hydrogenerator and consequently was not taken into account in the simulations. The hull was set in a position defined as typical of the Jules Verne Trophy (heel, trim and sinkage). Figure 1 shows a side view of the geometry in dynamic position, the location of the hydrogenerator is circled, the daggerboard is shown here only for information purpose.

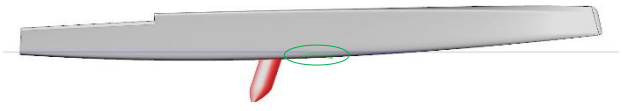

Figure 1 - Side view of the geometry

2.2 CFD SOLVER

The solver used for the study was ISIS-CFD, a RANSE free surface solver developed by École Centrale de Nantes and using Menter's k-ω SST turbulence model.

2.3 SIMULATION HYPOTHESIS

The major hypothesis made during this study was that the hydrogenerator would always be located below the free surface location, so that monofluid computations were performed. As a consequence, the trimaran was considered as a fixed body, sailing on calm water. Neither free surface effects, nor variations of mass flow rate in the device (due to waves and changes in the trimaran's dynamic behaviour) were taken into account.

2.4 NUMERICAL MODEL SETUP

2.4.1 Simulation domain and boundary conditions

Figure 2 shows a view of the simulation domain. A symmetry plane boundary condition was set on the top face of the domain (in white), located at z=0 m (free surface), a constant pressure condition was used on the outlet (in blue), and velocity inlets on the other faces (in red).

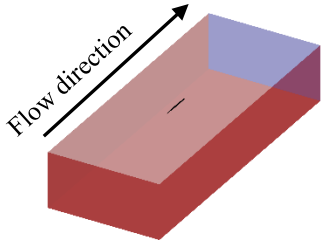

Figure 2 - Simulation domain

Figure 3 shows the hydrogenerator as it is installed in the hull, set in position in the simulation domain. The figure also presents the coordinate system used. x-axis is oriented towards the bow, z-axis is oriented up and y-axis is oriented to portside. The origin is located at the intersection of the symmetry plane (z=0) and the transom.

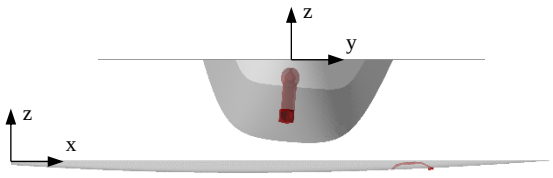

Figure 3 - Views of the hydrogenerator and the hull in the domain

2.4.2 Setup of a specific actuator-disk model

Since the turbine's thrust and torque influence the flow in the pipes, its effect needs to be modelled during the design process of the duct, in order to properly account for interactions between the duct design and turbine generated flow. However, the design of the turbine itself depends on the flow inside the duct and inversely. That's why an actuator-disk model was used at the beginning of the project, when iterating on the design of the duct. An actuator-disk is a virtual disk in which forces are applied on the flow. This model allowed to take into account for pressure losses and rotational effects created by the turbine. Based on such an approach, the choice of the right design of the duct could be made. Later on, based on the CFD simulations performed and results obtained, the turbine could be designed with the proper wake field in the duct.
Classically a turbine is designed and optimized for a particular operating point, which corresponds to a value of boat speed (kts) and rotational rate (rpm). Here, the designed was performed for a design speed of 25 kts, but computations were performed to assess the hydrogenerator's performances at 15 kts and 35 kts, which covers the speed range of the trimaran.

A specific actuator-disk (AD) had to be set up to accurately model the particular thrust and torque distribution in the duct.
Watt&Sea provided simulation data of the repartition of thrust (T) and torque (Q) over non-dimensional radius (r/R_{out}) (cf. Figure 4). Values are zero for r/R_{out} below 0.5611, that is, inside the shaft. These values were interpolated with 6th-order polynomial functions, made non-dimensional and normalized so as to be written as radial and tangential repartitions which were imposed during the computations through a dynamic library.

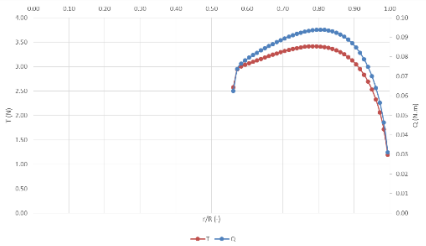

Figure 4 - Thrust and torque repartition of the specific AD

2.4.3 Pre-dimensioning

In order to determine the amount of thrust and torque to apply to the AD, a pre-dimensioning was made.
As mentioned, the goal is to have 300 W of useful power at 25 kts. Considering the electrical efficiency and the losses of heat energy due to the friction of the seals of the turbine on its shaft, this lead to consider a shaft power of 380 W, for a rotation rate of 1100 rpm. This is resumed by the following formula:

$$P_u=\eta_e\,(P_s - 2\,\pi\,n\,\alpha)$$

where η_e=0.83 is the electrical efficiency and α=0.15 N.m is the frictional torque between plastic and steel.
The turbine's torque is directly linked to the shaft power and rotation rate by the relation:

$$P_s=2\pi\,n\,Q_{turb}$$

Then, the thrust is linked to the shaft power through the hydraulic efficiency η_h and mean velocity in the duct:

$$P_s=\eta_h V_{turb} T_{turb}$$

At this stage, the mean velocity in the duct V_{turb} and the global efficiency are unknown. Hypothesis have to be made on their values. Based on Watt&Sea's experience on similar turbines, the global efficiency was assumed to be 0.65 and the mean velocity in the duct 4.8 m/s, corresponding to a mass flow rate of 46.4 kg/s based on the radius of the input pipe of 40 mm.
So, at the speed of design (25 kts), the imposed thrust and torque chosen were T_{AD}=121.8 N and Q_{AD}=-3.3 N.m.

2.4.4 Grid independence and y+ adaptation

Unstructured meshes were generated with Hexpress. A grid independence study was performed on three grid densities on the first geometry of the duct. The three meshes counted 4.6, 5.6 and 10.6 million cells. The $y+$ values inside the duct are above 30 for the coarse grid, and below 1 for the two others. On the hull, $y+>30$ was set for all grids, thus wall functions are used.
The grid independence study was based on the comparison of drag, mass flow rate, mean velocity in the actuator-disk centre and pressure and velocity fields.
This lead to choose the finest grid, with 10.6 million cells and $y+<1$ in the duct. Views of the mesh are presented on Figure 5.

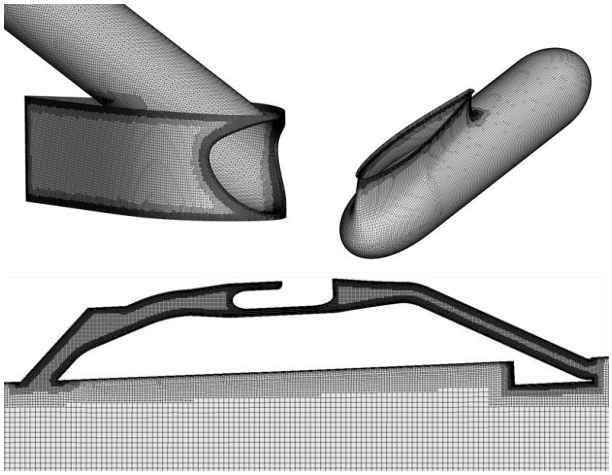

Figure 5 - Views of the surface and volume mesh adopted

3 DESIGN OF THE DUCT

Three designs of the duct were evaluated in CFD and compared on three main criteria: the mass flow rate at the turbine location, the additional drag generated by the whole device and the uniformity of the flow in the turbine disk (wake field).

3.1 GEOMETRIES OF THREE DESIGNS OF DUCTS

As it can be seen on Figure 6, the differences between the three designs of the duct, are mainly on the divergent pipe at the entrance, the entrance angle of the pipe relatively to the hull bottom line and the shape and angle of the exit pipe. The length of the shaft (red) was also 30 mm smaller for designs 2 and 3 than design 1. Finally, the top edge of the scoop of design 3 was flush to the hull keel line, whereas there was a small thickness for designs 1 and 2.
Some dimensions however, remained unchanged between the designs: the chord of the scoop, its thickness, the diameter of the inclined entrance pipe and the diameter of the main pipe, containing the shaft and generator device.

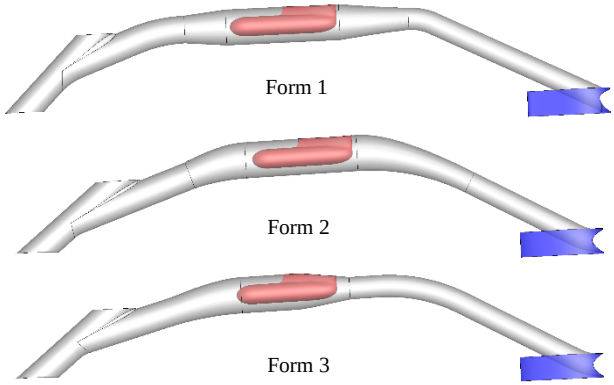

Figure 6 - Three designs of the duct: designs 1, 2 and 3

3.2 DRAG COMPARISON

The total drag (in kg) of the hydrogenerator was measured by adding the following contributions: the hydrodynamic drag computed in CFD, the drag due to the AD thrust, the drag due to the water carried in the device and the drag due to the mass of the device (estimated at 30 kg). The ratio used to convert a mass in hydrodynamic drag is 1/9.5. Table 1 lists all these contributions and presents the additional drag compared to the drag of the maxi-trimaran at 25 kts (3000 kg).

	Hydrogen.	AD	Water	Mass	Tot.	Diff. /Boat
Design 1	23.7	12.4	1.9	3.2	41.1	1.4%
Design 2	21.6	12.4	2.1	3.2	39.3	1.3%
Design 3	26.8	12.4	1.7	3.2	44.1	1.5%
diff. 2/1	*-8.8%*	*0%*	*10.5%*	*0%*	*-4.4%*	/
diff. 2/3	*24.1%*	*0%*	*-19.0%*	*0%*	*-10.9%*	/

Table 1 - Drag results for designs 1, 2 and 3

Design 2 presents the lowest drag of the three designs: it is 4.4% lower than design 1 and 10.9% lower than design 3. This is mainly due to the geometry of the divergent pipe, going from the scoop to the shaft. The changes in diameter and curvature are smoother than for designs 1 and 3, thus pressure losses are lower.

3.3 MASS FLOW RATE COMPARISON

Averaged values of velocity in a disk normal to the pipe and locate at the turbine's centre (which corresponds to the AD centre) enabled to compute the mass flow rate in the hydrogenerator. Values are listed in Table 2.

	V_{AD} (m/s)	Q_m (kg/s)
Design 1	5.1	49.3
Design 2	5.7	55.1
Design 3	7.2	69.6
diff. 2/1	*11.8%*	
diff. 2/3	*-20.8*	

Table 2 - Velocity and mass flow rate results for designs 1, 2 and 3

All designs have higher mass flow rate than the value chosen for pre-dimensioning (46.4 kg/s), so this was done in a conservative manner. Design 3 has the highest mass flow rate (+26.3% compared to design 2 and +41.2% to design 3). This happens because there is no divergent part on the entrance pipe, the diameter is constant until the shaft.

3.4 PRESSURE AND VELOCITY FIELDS COMPARISON

The comparison of pressure and velocity fields shown in the following figures help to understand the differences in drag and mass flow rate.

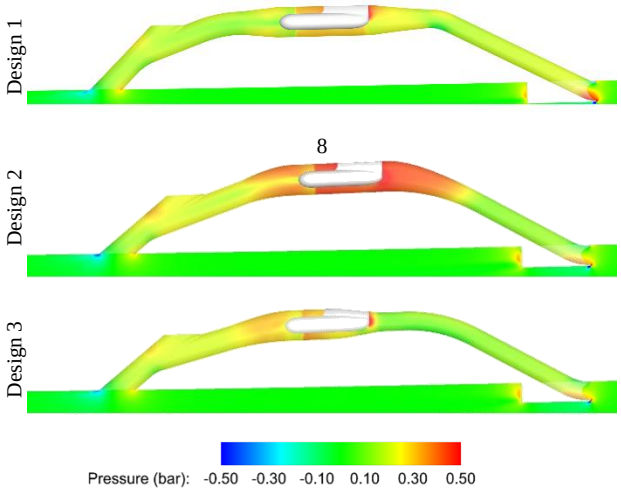

Figure 7 - Pressure field (bar) for designs 1, 2 and 3

The high pressure zone due to the actuator-disk presence (thrust force) is well visible around the shaft, it even goes forward up in the pipe for design 2, where the change in the pipes' diameter is the smoothest. The entrance pipe near the scoop presents also a high pressure zone in its bottom. This high pressure zone is bigger for design 1 because the angle of the pipe with the horizontal is steeper than for the other designs.

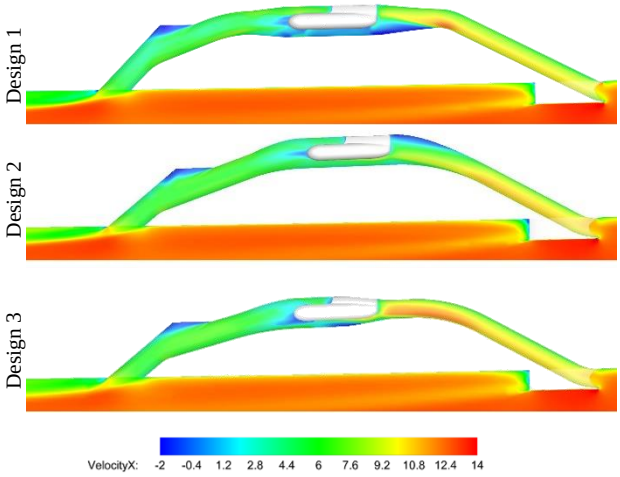

Figure 8 - Axial velocity field (m/s) for designs 1, 2 and 3

On Figure 8, zones of negative velocity are visible for all designs, especially on the top part of the exit pipe and around the shaft location. For designs 1 and 3, high recirculation zones occur below the shaft and in its wake. This effect is much more limited on design 2 where the recirculation is limited at the top of the divergent, in front of the shaft mast.

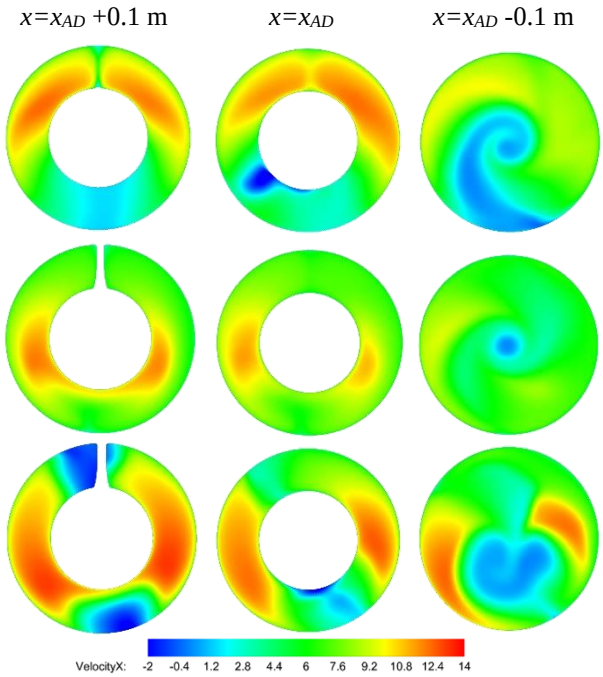

Figure 9 - Wake field maps (m/s) for designs 1, 2 and 3

From the simulations, wake field maps (transverse section at the location of the propeller and +/-0.1 m from this position) could be computed. These maps are shown on Figure 9, where the high variations of velocity across the section is highlighted. For designs 1 and 3, red zones, i.e. with high velocities are much larger than for design 2. On design 2, no negative velocity zone (blue) is visible, contrary to designs 1 and 3. It can be seen that design 2 presents the most uniform wake field map. It is an

important criterion to focus on since the wake field map is essential for the design of the turbine: the variations of velocity in that disk impact directly linked to the angle of attack of the fluid on the blades and consequently the turbine performances.

3.5 CHOICE AND EVALUATION OF THE FINAL DESIGN

3.5.1 Presentation of the final design

As it was explained in the previous chapters, the choice of best form was based on the total additional drag and the quality of the flow at the location of the turbine. The previous comparisons showed that design 2 has the lowest drag, an averaged mass flow rate and the most uniform wake field map .Thus this design was chosen as the base design for the final design of the hydrogenerator duct.
Only minor changes were made on the geometry: the scoop was made flush to the hull keel line, the convergent pipe after the shaft was slightly modified and the overall system was slightly elevated to be properly integrated in the maxi-trimaran.
Figure 10 presents the final design of the duct.

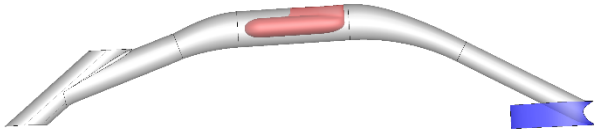

Figure 10 - Final design for the duct

3.5.2 Evaluation of the final design at different speeds

The final design of the duct was evaluated with an actuator-disk model for two extra flow (boat) speeds, 30 and 35 kts. The idea was to evaluate the influence of boat speed on the wake field map, so as to ensure the turbine designed could operate well at speeds higher than the design speed of 25 kts. Table 3 lists the values of mean velocity in the duct and mass flow rate for the three boat speeds.

	V_{AD} (m/s)	Q_m (kg/s)
25 kts	5.5	53.1
30 kts	7.1	68.6
35 kts	8.5	82.1
diff. 30/25	*29.1%*	
diff. 35/25	*54.5%*	

Table 3 - Velocity and mass flow rate results for final duct

For an increase of boat speed of 20% at 30 kts (resp. 40% at 35 kts), the increase in mass flow rate is 29% (respectively 54.5%), and so the hydraulic power available in the duct.

Figure 11 presents the velocity wake field maps but now decomposed into three main components: axial, tangential and radial velocities. The values are non-dimensional, based on the upstream speed.

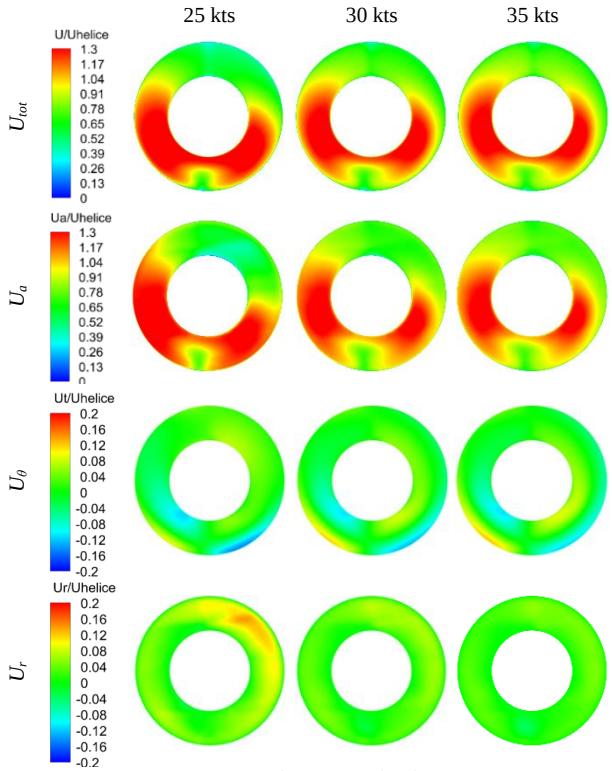

Figure 11 - Wake field maps for final duct

Two main comments can be made: first, the influence of boat speed on the wake field map is quite small: it slightly modifies the velocity field near the outer part of the duct. Then, the radial and tangential velocities are negligible compared to the axial velocity (different scales are used): this is a good point for the design of the blades of the turbine because this means the turbine will work similarly for a range of boat speed from 25 to 35 kts.

4 DESIGN OF THE TURBINE

4.1 PRESENTATION OF THE DESIGN TOOL

4.1.1 OpenProp general presentation

The propeller design relies on a numerical model developed according the lifting line theory devised by Prandtl for wings and Betz for propellers.
Such a model has been recently developed by Epps et al. and proposed to the public as a tool named OpenProp [1]. This software uses a vortex-lattice lifting-line representation of the blades with constant-diameter helical vortices to represent the blade wake. The code has an analysis capability to estimate the performance curve of a given design for use in off-design evaluation.
This tool can achieve very good results on open water propellers designs where several 3D empirical corrections are available and complete well the lifting line theory simplifications. The tool is also capable of open water turbines calculations. However, there is a lack of exhaustive studies done in this field to correct the 3D-

effects, even if academic studies have shown a fair agreement between results and towing tank tests.

4.1.2 Development of a specific model for turbines in hydrogenerators

The model developed in this study uses an adaptation of the above code mentioned with major modifications to account the forced-flow situation and the hydrogeneration case. First, an additional numerical loop forces the mass-flow to the value specified by the user, and the pipe and hub are modelled by symmetry conditions to maintain a purely axial flow on the walls.
Secondly a new case of optimisation scheme has been developed: the hydrogeneration model. This case differs with the initial one in OpenProp in terms of goals: the turbine case classically aims to maximise the energy recovered from the flow whereas the hydrogeneration case wants to target a determined shaft-power along with the lowest achievable drag. This nuance is critical for the forced flow situation where the head or inlet pressure are unconstrained and the fluid power potentially infinite. This difference has been implemented as a new case in the code, separate from propeller and turbine cases, pressure drop and drag are results of the optimisation loop.
The blade is modelled by a line divided into equal segments. At each point a circulation amount will be computed and later translated into a real airfoil section with its specific chord, pitch and camber.

4.2 DESIGN PROCEDURE OF THE BLADE

The design procedure of the blade unfolded in several steps.
In the first step the following input data were received:

- the flow velocity across the turbine. It was based on CFD's wake field maps which were simplified by annulus-averaging
- the rotation rate which is determined according to the electrical generator
- the number of blades
- the foil section type and mean line type
- the torque target (or shaft-power target)

According to this data, the model computed the optimum circulation that describes an ideal propeller answering the problem. The computation was done by iterations and convergence was achieved in less than 20 steps. After the optimisation routine, the circulation Γ was computed for each section of the blade.

In the second step, the chord law and lifting coefficients were calculated to ensure the circulation formula:

$$CL\ c = 2\ \Gamma / V^*$$

where CL is the section lift coefficient, c the section chord length, V^* the local inflow velocity and Γ the amount of circulation.

Then, in the third step, the thickness law was added. In OpenProp propeller routines, the thickness law and number of blades are used for empirical corrections on the pitch and camber to account to acceleration of the flow due to the thickness of the blades [2]. Equivalent correction has been integrated by Watt&Sea in this study, based on observations from on its hydrogenerators and experience on that matter.
Steps two and three allowed the manual control on the final shape and are useful to account secondary design criteria: mechanical resistance, cavitation-free operation and machinability
In the fourth step, the rake and skew laws were finally added, since they are not taken into account in the lifting line model. They are known to have insignificant effect in uniform flow and can also be arbitrary chosen by the designer according to secondary design criteria: level of non-uniformity of the real flow and mechanical resistance of blades. At that stage, the full geometry of the turbine was determined and checked off-design. A panel mesh of the geometry is presented on Figure 12.
Finally in step five, the off-design curves of the propeller were computed for a range of tip-speed ratios determined by the user as well as for different feathering angles (cf. Figure 17). A cavitation map was also computed for each off-design point to foresee the risk of cavitation. In this routine, each section of the blade was meshed and the local pressure evaluated thanks to VLM (Vortex Lattice Method).

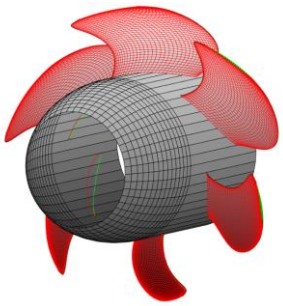

Figure 12 - Panel mesh of the six-blade turbine

5 FINAL VALIDATION OF THE HYDROGENERATOR

This section presents the results of CFD computations on the hydrogenerator with the rotating turbine. It compares CFD power predictions to the estimation of VLM.

5.1 SLIDING MESH SETUP

The simulations of rotating turbine are performed using the sliding grid method. In this technique, two domains are set in the computation: the background domain, containing the hull and the ducts is fixed, and a rotating domain containing the blades of the turbine and a part of the hub. These two domains are linked with sliding interfaces, they enable the solver to compute the flow going from one domain to the other.

Figure 13 presents views of the mesh of the turbine, the blades are highly refined, the target y+ is below 1; total mesh size is 19 million cells.

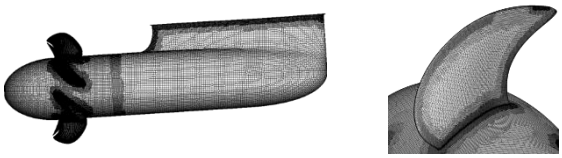

Figure 13 - Views of the mesh on the turbine and one blade

5.2 COMPARISON WITH ACTUATOR-DISK

The following figures present the comparisons between the rotating propeller simulation and the one performed with a simplified actuator disk model. It is interesting to see on the following figures that the pressure, velocity and wake field maps match pretty well between the computations with AD and rotating turbine. The major differences observed are on the wake of the turbine, just after the hub cone.

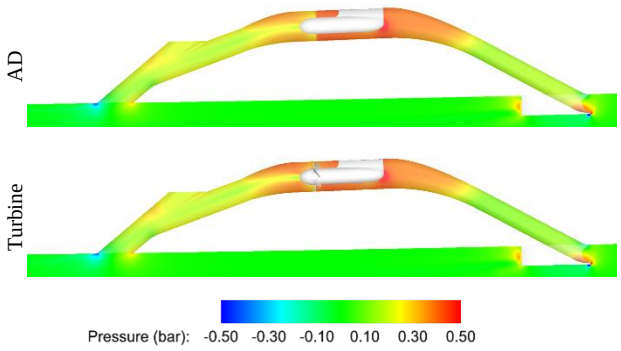

Figure 14 - Pressure field (bar) for AD and rotating turbine

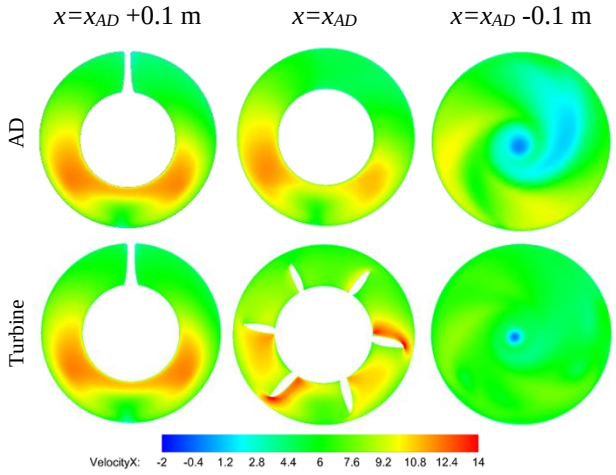

Figure 15 - Wake field maps (m/s) for AD and rotating turbine

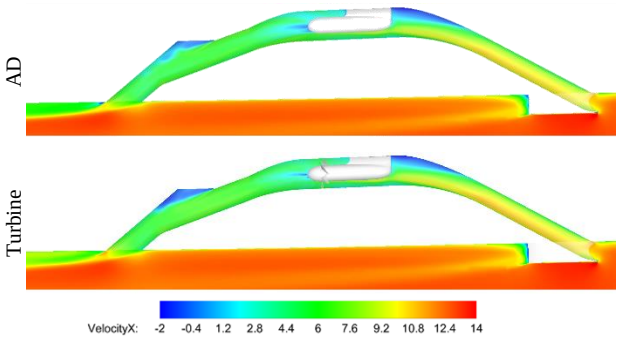

Figure 16 - Velocity field (m/s) for AD and rotating turbine

5.3 FORCES AND SHAFT POWER

The curves plotted on Figure 17 compare the performance coefficients predicted by VLM and the results of CFD on the three operating points (15 kts - 500 rpm; 25 kts - 1100 rpm; 35 kts - 1900 rpm).

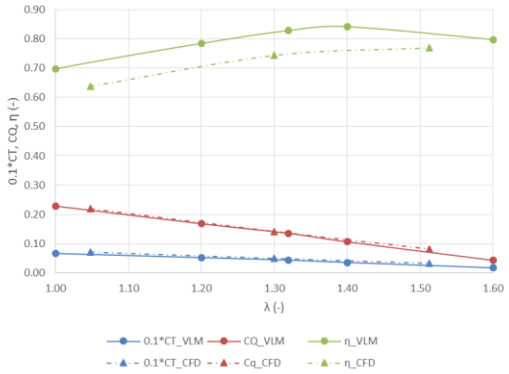

Figure 17 - Comparison of CFD and VLM performance curves of the turbine

The drag predicted by VLM is between 10 and 19% lower than CFD results and the torque is 2 to 13% lower. Therefore, VLM's computed efficiency is overestimated by 9% to 12% in comparison to CFD. Considering that VLM theory uses annulus-averaged velocities whereas the wake field is highly non-uniform, the agreement is quite good.

Concerning the evolution of shaft power over boat speed, CFD results predict 92 W at 15 kts, 410 W at 25 kts and 901 W at 35 kts.

Finally, the additional hydrodynamic drag of the hydrogenerator was evaluated for each operating point and compared to the trimaran's drag. The device adds around 1.2% drag at 15 kts, 1.5% at 25 kts and 2.1 % at 35 kts. These values are representative of the ideal case that would be steady state, on flat sea and are presumed to be less in normal sailing conditions, where the waves and pitch variation add important contribution to the total drag.

6 INSTALLATION AND SEA TRIALS

This sections presents how the hydrogenerator was custom built by Spindrift racing Team, then integrated to the trimaran and finally tested during sailing. A comparison between trials measurements of useful power and CFD estimations is presented.

6.1 INTEGRATION AND STRUCTURAL DESIGN

The system was designed to be fully retractable and watertight. The scoop can retract into a cassette, so that when it's in upper position, it is flush to the hull, and the aft pipe where the flow exits can be easily filled with a moving plug or piston. This enabled to reduce drag when the system is not running, stop charging when the batteries are full and to get an access to the hydrogenerator while sailing, for easier maintenance.

A structural study was made for the composite carbon parts in relation to water pressure on the hull and inside the pipe. Weight control was also important. Custom tooling was designed and machined to fit the pipe design and to ensure the best surface water interaction. It took 600 hours to build, assemble and integrate the hydrogenerator system into Spindrift 2's central hull.

Figure 18 presents a view of the retractable scoop and the hydrogenerator seen from inside the hull. Figure 19 shows the turbine blades manufactured in moulded design.

Figure 18 - View of the scoop and the hydrogenerator implanted on Spindrift 2

Figure 19 - Turbine realisation

6.2 ELECTRICAL DESIGN AND DATA LOGGING

The hydrogenerator creates a tri-phased tension (up to 40 V). A Watt& Sea MPPT converter was needed to ensure a stabilized voltage and current for the Li-Ion battery technology. From this converter, it's possible to get data from the hydrogenerator such as temperature, rpm, voltage, power etc.
Coupled with other data (such as sailing and battery charging) in an in-house data logger, theoretical predictions from CFD can be matched with real measurements.

6.3 TESTING AND RESULTS

Few sea trials were made in La Trinité-sur-Mer to check the kinetics, leaks etc. when sailing at high speed and in heavy seas. Interaction with the on-board electrical system, navigation instruments, etc. and the delivered power were checked as well.
Then, the transatlantic delivery to Quebec (Canada) during June 2016 was a good opportunity to test the system before the Québec to Saint-Malo race and a Jules Verne Trophy attempt.
From the delivery log, useful power versus boat speed can be plotted. On Figure 20 are shown the log dataset from sea trials (green triangles) and the three CFD points (blue dots).

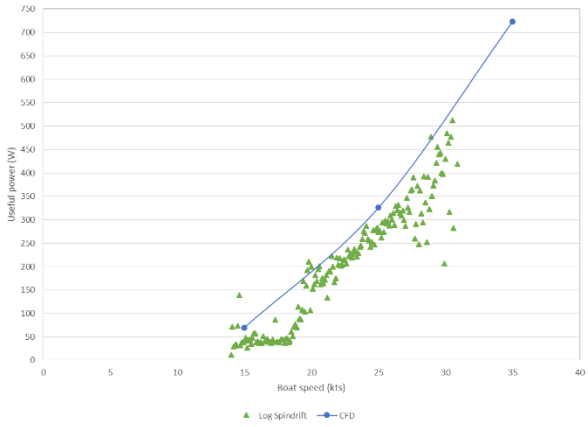

Figure 20 - Sea trials power data versus CFD estimations

First, important dispersion can be seen on the sea trials measurements, especially around 15 kts and above 27 kts. In a general manner, such dispersion is unavoidable on sea

trials because of difference of latency in recording instruments (here speedometer and converter).
Then, no measurements are available above 30 kts, thus no comparison can be made with CFD at 35 kts.
Between 20 and 26 kts, the measurements have less dispersion and their values follow the trend predicted by the numerical simulations (blue line).
Averaged values of measurements at 15 kts and 25 kts give respectively 38 W and 274 W of useful power. CFD estimations at these speeds were 70 W and 326 W; this represents around 46% and 16% less power than what has been effectively logged on Spindrift 2.

Indeed, the differences between CFD estimations and measurements can be explained by three main causes. First, the hypothesis made for the numerical study: only monofluid simulations were performed, and on calm water; which does not correspond to the reality of the sea trials where the trimaran is free to move, and interactions with the free surface exist, especially in heavy seas. Then, the differences between the real pipes built in composite and the CAD design, ideally smooth and regular, which was used in CFD, can also account for the observed discrepancies. Finally, the location of the system on the fore part of the hull lead the scoop of the hydrogenerator to be often out of the water due to the multihull pitch. Therefore, the hydrogenerator saw high fluctuations of the incoming flow and was not always fully immersed, so the turbine rotation rate was very irregular. This fact might account for the dispersion of measurements at high speed.

However, it should be noticed that, at the design speed of the turbine of 25 kts, CFD prediction differ only by 16% from the measurements, which is fairly good, given the above mentioned facts.

7 CONCLUSIONS

This paper presented the numerical study of design and optimisation of a ducted hydrogenerator for the maxi-trimaran Spindrift 2. CFD simulations enabled to design an optimized geometry of the duct in terms of mass flow rate, additional drag and uniformity of the wake field map. Then, the appropriate turbine was designed to fit the duct and to produce 300 W of useful power at 25 kts. Once built and integrated to the trimaran's central hull, the hydrogenerator was tested in sea trials by Spindrift racing team. Measurements of the output useful power were logged and showed that the values are close to the CFD predictions (16% difference at 25 kts).
Three improvements could be made to ensure higher efficiency of the hydrogenerator at lower boat speeds. First, moving the hydrogenerator further aft the hull (as the engine is not required during a record attempt for example), so that the scoop would be more often immersed in water, even when the trimaran is pitching bow up. Then, improving the surface quality and connections between the different composite parts of the pipe. And finally, set up variable pitch blades on the turbine, so as to change the angle of attack with the boat speed, to get higher rotation rate, and thus power.

REFERENCES

1. Epps et al., 'OpenProp: An Open-source Parametric Design and Analysis Tool for Propellers', 2010.
2. Eckhardt & Morgan, 'A Propeller Design Method', 1955.

AUTHORS BIOGRAPHY

L. Mazas holds the current position of Hydrodynamic & Project Engineer at HydrOcean. He is in charge of CFD studies on sailing yachts. His previous experience includes hydrodynamic studies on maxi-trimarans, foiling catamarans and IMOCA monohulls.

D. Barcarolo holds the current position of Senior Hydrodynamic & Project Engineer at HydrOcean. He is in charge of CFD studies on offshore industry. His previous experience in sailing yachts includes aerodynamic and hydrodynamic studies on foiling catamarans, maxi-trimarans and IMOCA monohulls.

Spindrift racing is a racing stable, based in the south of Brittany. It was founded by Dona Bertarelli and Yann Guichard in 2011. Spindrift racing runs a fleet of boats for several complementary projects including a M32 catamaran; a Decision 35 catamaran (Ladycat powered by Spindrift racing), and the 40-metre maxi-trimaran (Spindrift 2).

M. Michou holds the current position of CEO at Watt&Sea. He has been engineering hydrogeneration devices since 2007, mainly for sailing boats, with a global understanding approach; He has designed several internal tools to deal with specific hydro-generation needs from hydrodynamic codes to energy conversion devices.